Springer

KSME

Journal of Mechanical Science and Technology 28 (6) (2014) 1~10
www.springerlink.com/content/1738-494x
DOI 10.1007/s12206-013-0913-y

Self-powered piezoelectric energy harvester for bicycle †

Dejan Vasic[1,2,*], Yu-Yin Chen[1] and François Costa[1,3]

[1]*SATIE, UNIVERSud, ENS Cachan, 94235 Cachan, France*
[2]*Université de Cergy-Pontoise, Neuville/Oise, 95031 Cergy Pontoise, Cedex, France*
[3]*ESPE de Créteil, Université Paris Est Créteil, Place du 8 mai 1945, 93000 St Denis, France*

(Manuscript Received 000 00, 2013; Revised 000 00, 2013; Accepted 000 00, 2013)

Abstract

Various electronic accessories, such as on-board computers, communication devices, and wireless sensor nodes, have been installed on bicycles for several years. A powering scheme from ambient energy could avoid the use of batteries and improve the availability of these devices even when the bicycle is unused for a long time. This paper reports on vibration resources detected in a bicycle as a potential energy source for supplying these on-board devices. Measurements showed that the bandwidth of energy vibration is reduced with speed and that the vibrations at any location in the bicycle are nevertheless sufficient for useful vibration harvesting. For this application, a piezoelectric vibration harvester was designed and equipped with a voltage switching interface circuit. Sufficient energy is harvested during the field test.

Keywords: Bicycle vibration; Energy harvesting; Piezoelectric transducer; Self-powered SSHI interface

1. Introduction

Batteries or dynamos almost exclusively supply power to electronic devices on bicycles (e.g., digital displays, such as speedometers or communication devices). However, both power systems have disadvantages. When using dynamos, cyclists exert more effort than necessary to compensate for the friction that the dynamo creates, which is generally an important reluctant torque because of low-cost building. Moreover, the dynamo is often noisy for the same reason. The use of batteries is restrictive and not eco-friendly, particularly when several on-board devices are used. Bicycles are subject to environmental factors, such as mechanical loads and dynamical constraints, when being driven. Therefore, structural monitoring is required to increase bicycle lifespan [1]. Structural reliability control and critical state diagnostics can be achieved by using wireless sensors. The progress in low-power components has reduced electronic device consumption and enables self-powered autonomous electronic devices, including energy harvesters, to be supplied by mechanical vibrations. This progress opens the possibility for small generators to supply self-powered systems completely by producing sufficient power for low-consumption electronics. In the majority of applications, piezoelectric transducers convert mechanical energy from vibrations into electrical energy [2]. However, electromagnetic or electrostatic transducers can be also used in place of piezoelectric transducers [3-5]. Piezoelectric technologies have received considerable attention for their high electromechanical coupling and lack of a requirement for an external voltage source. Numerous studies on piezoelectric energy harvesting have been published since 2002. Tang et al. [6] and Khaligh et al. [7] performed a long synthesis and developed a state-of-the art design for vibration piezoelectric energy harvesting. Integration of power generators significantly extends the lifespan of embedded devices owing to advances in the efficiency of piezoelectric transducers and power electronics. However, total power budgets are low, typically below a few milliwatts. Therefore, power electronics designs are subject to tradeoffs. Circuit topologies are different for devices with high-power applications. Electronic devices used to increase electromechanical coupling must be totally self-powered, such that power consumption must be less than the harvested power.

In energy-harvesting applications, a piezoelectric element is attached to a host structure, whereas an electronic circuit is connected to the piezoelectric element. The electronic circuit converts the vibration energy of the host structure into electrical energy, after which the generated electrical energy is stored in a buffer. An impedance matching circuit is required to maximize the generated power because the piezoelectric element has a large intrinsic capacitance. An inductor can compensate for the piezoelectric clamped capacitor [8]. However, the inductor cannot adapt to environmental variations, and the inductance value becomes extremely large in a low

*Corresponding author. Tel.: +33 1 34 25 68 91, Fax.: +33 1 47 40 21 99
E-mail address: vasic@satie.ens-cachan.fr
† Recommended by Associate Editor

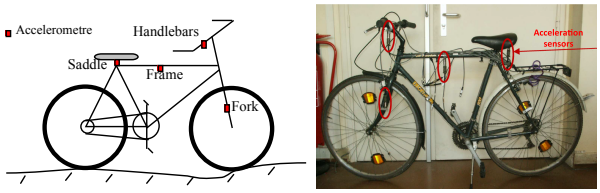

Fig. 1. Acceleration sensors mounted on a bicycle.

frequency range. To overcome this drawback, switching-type charging circuits have been proposed and widely used in recent years. In switching circuits, the switches are operated synchronously with the vibration of the host structure to optimize the power flow. Several synchronized switching circuit topologies and corresponding switching laws were proposed. These techniques boost the output power from the piezoelectric energy harvester [9-16]. The fundamental concept of switching-type electric interfaces (SSHI) technique is using the resonance between piezoelectric clamped capacitance and shunt inductance during a short time interval to inverse the piezoelectric voltage. The switching shunt circuit is only switched on at the extrema of the displacement or at the zero-crossing of velocity to shift the voltage phase across the piezoelectric element to optimize power flow.

In this study, we proposed the use of a totally self-powered piezoelectric energy harvester to improve the battery life of embedded devices on bicycles. Rolling-induced bicycle frame vibrations are promising ambient energy sources. However, no detailed data on bicycle vibrations are available in the literature. Acquiring vibration data is a serious, time-consuming, and expensive venture.

2. Bicycle vibrations

Estimating available mechanical energy by measuring and analyzing vibrations and frequencies is a necessary step in the development of bicycle piezoelectric generators. Measurements were performed at different locations in an experimental bicycle (Fig. 1) to identify where the maximum amount of energy harvesting was possible. A piezoelectric generator was then developed to identify the natural modes of bicycle vibration. Vibration sources of moving bicycles have multiple origins, but mainly stem from the irregularities of track rolling surfaces and the movement of the cyclists. These vibrations can also originate from tire treads and wheel imbalances. Therefore, different excitation frequencies can exist.

Acceleration sensors from Wilcoxon (784A) combined with a portable data acquisition unit from Swantek (SVAN 948) were used. This device features four channels, each of which a 20-bit A/D converter with a 51.2 kHz sampling rate. Four acceleration sensors were mounted on the bicycle (VTC Roadside Decathlon 500) at the following locations: fork, saddle, frame, and handlebars. Sensor sensitivity was 100 mV/g, and vertical acceleration was measured for the microgenerators. Different types of tracks and speed values

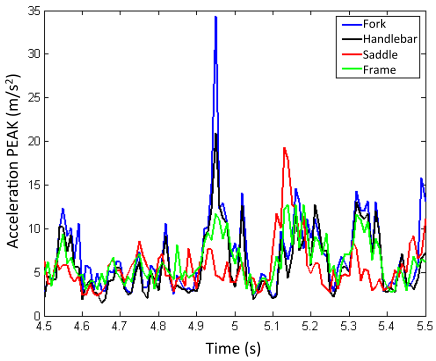

Fig. 2. Peak acceleration of vibrations at the fork, handlebar, seat, and frame as the bicycle rolls at 21 km/h on a cycle track.

were tested. The unit first recovers signals and then calculates acceleration peak value based on time interval T_b. The value is then stored in a buffer. Once the bicycle is instrumented, a series of measurements was conducted by imposing different almost constant cycling speeds. Fig. 2 shows the historical measurement signal peak sampled at 10 ms. When the bicycle is traveling at 21 km/h on a cycle track, the weight of the cyclist is approximately 60 kg. The peak value is defined as the maximum of the absolute value of the signal taken every 10 ms. The magnitude of the spikes in the time domain signal of Fig. 2 contains information about the track. The spikes of 35 m/s^2 measured at the fork are obtained when the front wheel crosses a hole, whereas the second spike of 20 m/s^2 measured at the saddle is obtained when the rear wheel crosses the same hole.

The frequency spectrum of the detected vibrations provides valuable information on the applicability of resonant or non-resonant harvesters. Fig. 3 shows two frequency spectra measured at four locations of the bicycle, one when the bicycle is rolling on a cycle track and another when the bicycle is rolling on a paved runway. The vibration amplitudes at the fork reach up to 2.5 m/s^2 at frequencies around 18.8 Hz, whereas the spectral amplitude at the saddle is less than 1.8 m/s^2. The maximum vibration amplitude corresponds to the resonance of the system, bike + rider + track. Such amplitude cannot be combined with the pedaling, which does not exceed 3 Hz to 5 Hz. Vibrations that appear within a few hundred Hz are attributed to the track and tires. The vibrations of the metallic frame of the bike are situated around a few kHz. The fundamental frequency changes with the bicycle speed. The maximum magnitude is observed at the same frequency for the four parts being tested.

The influence of different runway profiles, cycle track, and paved runway, as well as that of the bicycle speed, on vibration acceleration is investigated. The bicycle speed is measured by using an electronic tachometer. Fig. 4 shows the maximum amplitude of vibration as a function of bicycle speed in a cycle track and a paved runway. The amplitude of vibration is at the maximum at the handlebar or at the fork, whereas the acceleration always increases with bicycle speed.

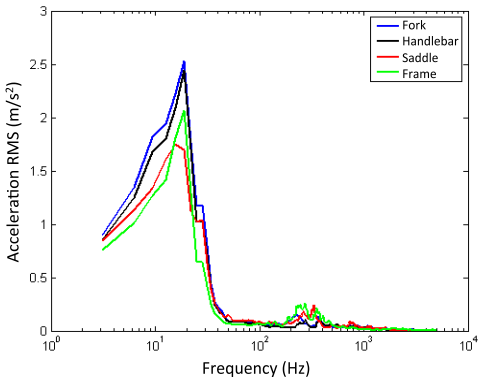

(a)

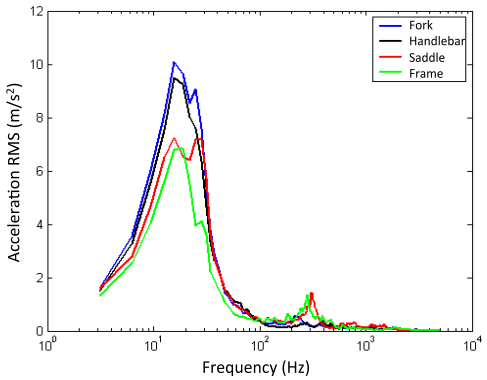

(b)

Fig. 3. Frequency spectra of bicycle vibration acceleration rolling at 21 km/h: (a) cycle track; (b) paved runway.

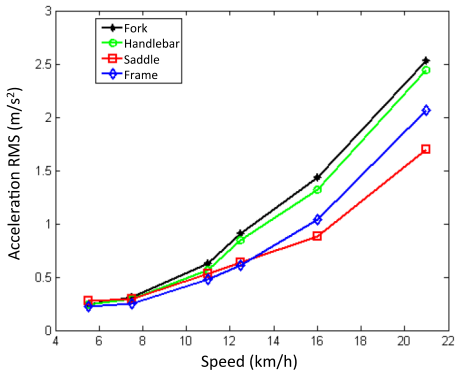

(a)

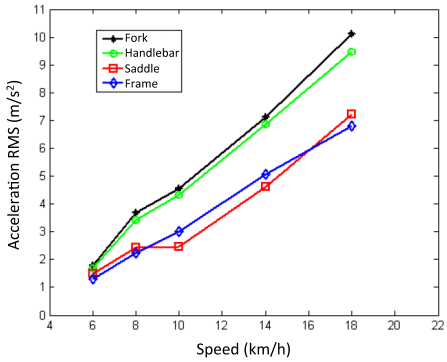

(b)

Fig. 4. Maximum vibration acceleration as a function of bicycle speed: (a) cycle track; (b) paved runway.

The vibration spectrum and sensor optimal location are insufficient information for the design of a piezoelectric microgenerator. The frequency bandwidth in which energy is concentrated is also important in the design of an energy recovery device. A frequency domain area containing over 80% vibration energy is defined. The square integral of the spectrum amplitude represents the energy level of the vibration signal, the energy of which is defined by Perceval's theorem (Eq. (1)), where t is time, and f is frequency. The vibration spectrum shown in Fig. 5(a) in the case of a bicycle rolling on a cycle track served as the basis for plotting the cumulative sum increasing in the frequency domain. The frequency range in which the energy is between 10 % and 90 % of the total is indicated in the plot.

$$\int_{-\infty}^{+\infty} |x(t)|^2 dt = \int_{-\infty}^{+\infty} |X(f)|^2 df \quad (1)$$

In the example of the fork vibration when the bicycle is rolling at 21 km/h shown in Fig. 5(b), 80% of the energy concentrates in the frequency band between 6.3 and 28.1 Hz. Frequency bands with high concentrations of vibration energy, common to all track types tested at various speeds, are generally between 12.5 and 28 Hz. Measured vibration levels remain low as acceleration reaches 10 m/s^2 in extreme rolling cases on paved runway.

Fig. 6 plots the previously presented speed conditions. These curves show the evolution of the fundamental vibration frequency, depending on the speed and on the frequency range for each speed in which 80% of the energy is located on the cycle track (dashed envelope curve). The frequency band of 80% vibration energy decreases when bicycle speed increases. Therefore, energy is concentrated around the fundamental vibration frequency as speed increases.

3. Energy harvesting device

An inertial harvester was used to search for electrical energy from vibrations. A typical harvester is composed of a cantilever beam with a tip mass at the end and a piezoelectric layer bounded on the beam with proof mass, which operates mainly around the first natural frequency [17]. A switching-type electric interface is adopted to optimize electromechanical conversion and to rectify piezoelectric voltage. A schematic diagram of our vibration harvester with the electric interface is shown in Fig. 7. The interface is composed of a bi-directional switch K and an inductor L in series with the piezoelectric element and the rectifier. Switch K is in an open-

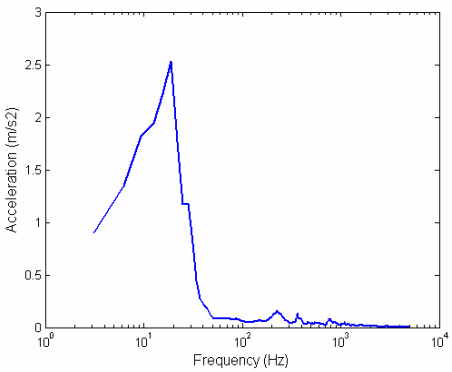

(a)

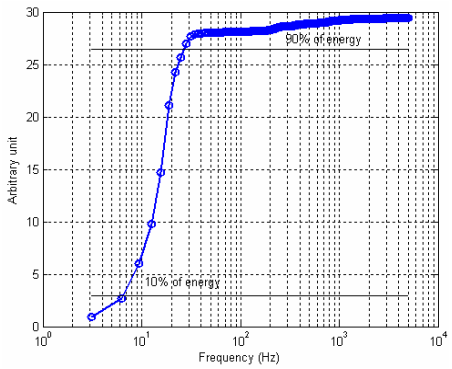

(b)

Fig. 5. (a) Frequency spectrum of vibration at the fork on a cycle track at 21 km/h speed; (b) energy repartition: cumulative sum of the acceleration squared.

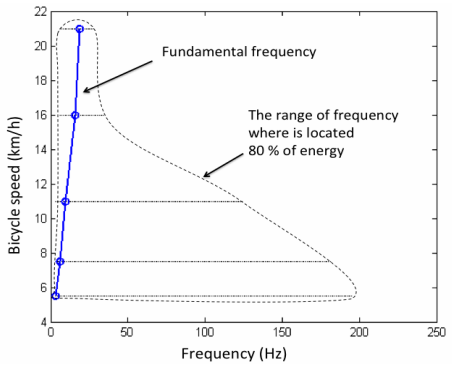

Fig. 6. Bicycle speed as a function of fundamental vibration frequency and the range where 80% of the energy is located.

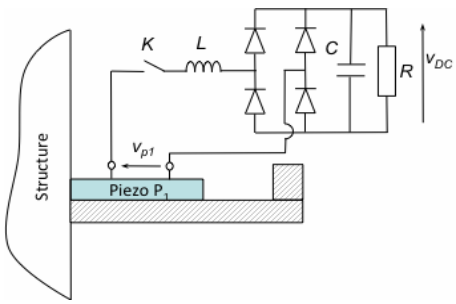

Fig. 7. Schematic diagram of vibration harvesting with electric interface SSHI.

Fig. 8. Harvester with piezoelectric layer and tip mass.

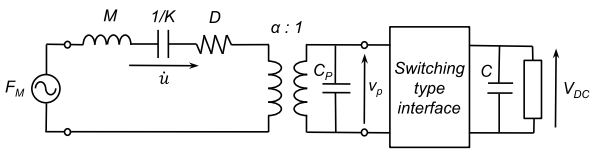

Fig. 9. Equivalent electric circuit of the single-mode piezoelectric switching shunt damping technique.

circuit state most of the time. Switch *K* conducts energy transfer for only short periods. An image of the harvester is shown in Fig. 8. The piezoelectric material used is PZT. The natural resonance frequency of the harvester is 18.8 Hz. This frequency was chosen because it was optimal for a bicycle speed of 21 km/h when the maximum energy is concentrated around the resonance frequency. A tip mass (m = 5.32 g) placed at the end of the beam is used to adjust resonance frequency to 18.8 Hz.

3.1 Electromechanical model

The governing equations of a piezoelectric element can be expressed as (2) and (3) [18].

$$F_P = K_P^E u + \alpha v_P \tag{2}$$

$$I = \alpha \dot{u} - C_P \dot{v}_P \tag{3}$$

where F_P is the external force exerted on the piezoelectric element, I is the outgoing current generated from the piezoelectric element, K_P^E is the short-circuit stiffness, α is the forced-voltage coupling factor, C_P is the static capacitance of the piezoelectric element, and u is the system displacement.

A mechanical model based on a spring-mass system provides a good description of the vibration behavior near the resonance of the host structure. Therefore, this system, which is composed of the beam and the piezoelectric patch, can be modeled simply as a one degree-of-freedom system of mass M, spring K^E, and damper D. According to the dynamics equation, the differential equation of this electromechanical system where the response to the external force F_M is described by Eq. (4):

$$M\ddot{u} + D\dot{u} + K^E u + \alpha v_P = F_M \tag{4}$$

Eqs. (3) and (4) can serve as bases to establish the equivalent electric circuit of the beam, as shown in Fig. 9. In this

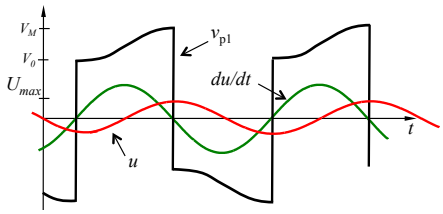

Fig. 10. Waveforms of SSHI interface.

figure, $\dot{u}$ represents the velocity of the host structure at a particular location, which also can be considered as the current in the equivalent circuit, and v_p is the voltage across the piezoelectric element. v_p is directly called piezoelectric voltage for simplicity.

3.2 Electric interface

The switching-type electric interfaces called SSHIs were widely developed over the past decade to improve the output power of piezoelectric elements. This technique optimizes electromechanical energy conversion by changing the waveform of the piezoelectric voltage. The piezoelectric voltage is a key parameter for optimizing the power flow P, as shown in Eq. (5).

$$P = \frac{1}{T}\int_0^T \alpha\, \dot{u} v_P dt \tag{5}$$

where T represents the vibration period (i.e., $T = 2\pi/\omega$). Piezoelectric elements and structures are usually weakly coupled in energy harvesting applications, which indicates that energy extraction from piezoelectric elements does not disturb the vibration behavior of the structure, and the magnitude of velocity $\dot{u}$ can be assumed to be unchanged. In this case, power depends only on two factors, namely, the phase between voltage v_P and velocity $\dot{u}$, as well as the piezoelectric voltage amplitude. Hence, voltage v_P and velocity $\dot{u}$ need to be in phase, and voltage amplitude needs to be increased to achieve good power output performance.

The schematic diagram of the SSHI in series configuration is shown in Fig. 7. Fig. 10 shows the corresponding key waveforms. When the local extreme displacement or zero vibration velocity occurs, switch K is switched on for a very short period. Within this period, the clamped capacitor C_P of the piezoelectric element resonates with inductor L, and the piezoelectric voltage v_P inverses. Accordingly, the SSHI circuit increases the magnitude and places the piezoelectric voltage v_P in phase with vibration velocity, which indicates that more energy is extracted from the vibration source. The results also show that the energy stored in the structural clamped capacitor C_P is extracted by the LC resonance circuit, such that the piezoelectric voltage is increased [19-21]. SSHI technique enlarges the coupling factor in the weakly coupled structure [22]. A full bridge rectifier is used to convert AC voltage to DC voltage for storage buffers.

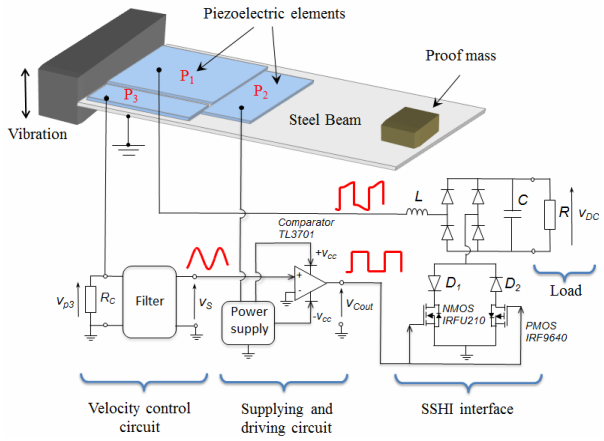

Fig. 11. Schematic diagram of the energy harvester with self-powered SSHI interface.

The output power P_{SSHI} of the piezoelectric energy harvester with SSHI interface is given by [15]

$$P_{SSHI} = \frac{\omega_0 \alpha^2}{2\pi C_P}\frac{1+q_{LC}}{1-q_{LC}}U_{max}^2 \tag{6}$$

where $q_{LC} = \exp(-\pi / 2Q_{LC})$ is a function of the quality factor Q_{LC} of the resonant LC_P circuit, and U_{max} is the displacement magnitude.

4. Self-powered electric interface for energy harvester

The circuit requires a power source to supply the electronics because of the use of switches in the SSHI interface [23-26]. Part of the extracted energy is used to design a totally self-powered device. Moreover, given that the approach is a synchronous technique, the displacement or the velocity must be measured accurately to obtain the driving signal for the switches. The technique used in this work divides the piezoelectric element into three parts. The largest part, called P_1, behaves in a manner similar to the conventional piezoelectric element used for the main energy harvesting and is connected to the SSHI and the rectifier. The second piezoelectric element, called P_2, is a smaller patch that works in a manner similar to an energy-harvesting device to provide the power supply to the driving electronics. The third piezoelectric element, called P_3, is a smaller patch designed to sense the velocity and to generate the driving signals used to control the switches at the optimal times. A schematic of the overall circuit is shown in Fig. 11 with the functions of different sub-circuits labeled. The system will be analyzed in detail in the following subsection.

4.1 Zero-velocity crossing detector (piezo-element P_3)

Fig. 12 shows the electric circuit and the theoretical waveforms of the zero-velocity crossing detector. The mechanical

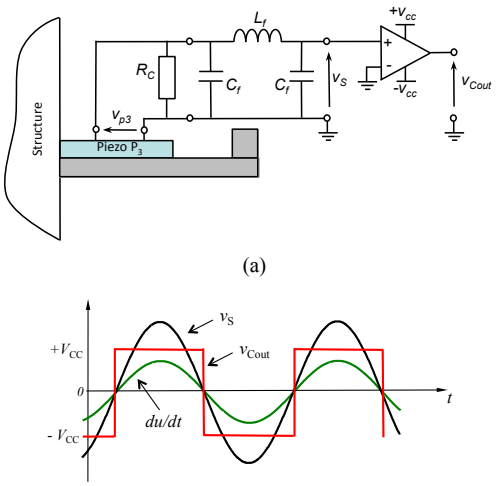

Fig. 12. Velocity zero crossing detector: (a) electric circuit; (b) theoretical waveforms.

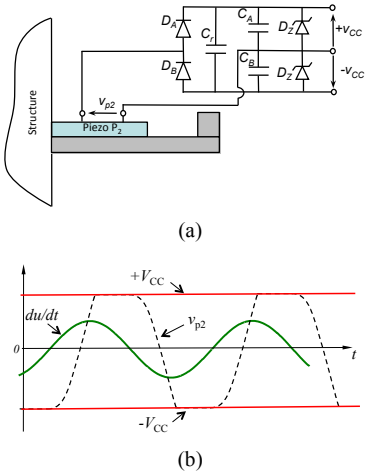

Fig. 13. Power supply circuit: (a) electric circuit diagram; (b) key waveforms.

current in the electric equivalent circuit of a piezoelectric element can be assumed to be velocity. Thus, if the output terminal is short circuited, the current through this short circuit is proportional to velocity, that is, $i_{sh} = \alpha \dot{u}$. To convert this current into voltage, this short circuit can be realized by a small value of resistance. Thus, the voltage across the shunt resistance represents the velocity of the structure. The value of the current-sensing resistance R_C must be significantly smaller than the output impedance of the piezoelectric patch. As shown in Fig. 12(b), the velocity signal (black curve) phases with the output current (green curve). To avoid noise problems, a low-pass filter should be used because voltage inversion introduces high-frequency vibrations into the system. A third-order low-pass filter is used. This filter is composed of two capacitors and an inductor. The filter ensures that high-frequency noise is sufficiently reduced to generate accurate control signals with minimum phase lags to maintain the efficiency of the SSHI technique. Finally, voltage v_s at the output of the filter is connected to a comparator, the output v_{Cout} of which is used to drive the switches, as shown by the red curve in Fig. 12(b).

4.2 Power supply (piezo-element P_2)

Fig. 13 shows the electric circuit and the theoretical waveforms of the power supply. This circuit provides two DC voltage sources, $+V_{CC}$ and $-V_{CC}$, to supply the comparator and the switches of the electric interface. The power supply circuit is composed of two diodes (D_A and D_B) and three capacitors (C_A, C_B, and C_r). The two diodes work as rectifiers to charge the capacitors. Capacitor C_A smoothens the positive voltage between V_{CC} and the ground, whereas capacitor C_B smoothens the negative voltage between $-V_{CC}$ and ground. Capacitor C_r smoothens the voltage between V_{CC} and $-V_{CC}$. Two Zener diodes D_Z are used to limit excursion and to regulate the DC voltage. The two regulated voltages, V_{CC} and $-V_{CC}$, are connected to the comparator. The output of the comparator is used to drive the switches. The comparator used in this application is a nanopower comparator TL3701 from Texas Instruments that sinks a small and constant current (I_{Comp} = 560 nA) for DC voltage V_{CC} higher than 2.5 V.

5. Experimental results and discussion

The characterization of the piezoelectric energy harvester on a bicycle traveling outdoors is feasible but impractical because of poor reproducibility (irregular velocity, random profile runway). This characterization requires the testing of different load values; for example, a series of resistance values and measurements of the voltage produced to deduce the corresponding power. Therefore, we performed the characterization differently: one indoors and another on a test bench. A shaker simulates the vibration source. Vibration frequency and amplitude are matched closely with the bicycle characteristics (at the frequency in which the maximum acceleration is found). This frequency is approximately 18.8 Hz in reference to the frequency band defined above.

5.1 Experimental setup

Fig. 14 shows the experimental setup and images of the zero-velocity crossing-based series-SSHI interface. The experimental structure is a cantilever steel beam with three 31-type PZT-QA elements provided by the Eleceram Technology Co., Ltd. A shaker excites the fixed end of the beam, and a DAQ card (NI USB-6259) on a notebook computer generates a shaker-driving signal. A CCD laser-displacement sensor (Keyence LK-G32) is used to measure the beam tip displacement. The NI DAQ card records the piezoelectric voltage, displacement, and acceleration. Table 1 shows the cantilever

Table 1. Dimensions of the electromechanical transducer.

	Length × Width × Thickness
Steel beam	83 mm × 26 mm × 0.25 mm
Piezoelectric patch P1	38 mm × 16 mm × 0.3 mm
Piezoelectric patch P2	21 mm × 15 mm × 0.3 mm
Piezoelectric patch P3	35 mm × 5 mm × 0.3 mm

Table 2. Model parameters obtained by measurement.

Symbol	Values	Definitions
f_{short}	18.77 Hz	Short circuit resonance frequency when piezoelectric element is in short circuit
f_{open}	18.8 Hz	Open circuit resonance frequency when piezoelectric element is in open circuit
δ	0.0105	Open circuit mechanical damping coefficient
C_{p1}	45 nF	Clamped capacitance of P_1
C_{p2}	23 nF	Clamped capacitance of P_2
C_{p3}	12 nF	Clamped capacitance of P_3
λ_1	1220 Vm^{-1}	Ratio between measured displacement and open circuit voltage
λ_2	674 Vm^{-1}	Ratio between measured displacement and open circuit voltage
λ_3	1123 Vm^{-1}	Ratio between the measured displacement and open circuit voltage

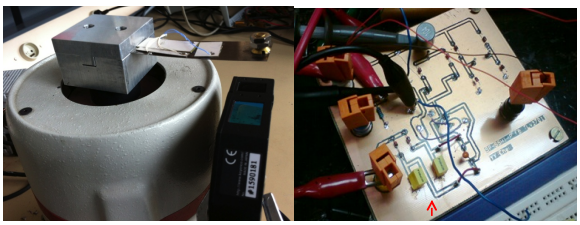

Fig. 14. Experimental setup and images.

beam dimensions and the piezoelectric elements. The size and clamped capacitance of the main piezoelectric patch are significantly greater than those of the two small piezoelectric patches.

Model identification followed the method proposed in [27]. Table 2 arranges the model parameters obtained based on the measurements near the first resonance. The tip displacement of the beam u was measured as the piezoelectric element was in open circuit and in short circuit. These measurements were calculated to obtain other model parameters, as shown in Table 3. The detailed relationships between the measurements and the corresponding model parameters are presented in the last column of Table 3.

The circuit connected to P_1 for SSHI is composed of several parts: an inductor L for LC resonance to enhance power; four Schottky diodes to confine current flow; load composed of a resistor and a capacitor; and an NMOS (IRFU210) and PMOS

Table 3. Model parameters calculated by measured data.

Symbol	Values	Definitions
k^2	0.0032	$k^2 = \frac{f_{open}^2 - f_{short}^2}{f_{short}^2}$
α_1	0.0000549 N/V	$\alpha_1 = \lambda_1 C_{P1}$
α_1	0.0000155 N/V	$\alpha_2 = \lambda_2 C_{P2}$
α_1	0.0000134 NV^{-1}	$\alpha_3 = \lambda_3 C_{P3}$
K	20.93 Nm^{-1}	$K = \frac{\alpha_1 \lambda_1}{k^2}$
M	0.0015 kg	$M = \frac{K}{4\pi^2 f_{short}^2}$
D	0.0037 $Nm^{-1}s^{-1}$	$D = 4\pi\zeta M f_{open}$

Table 4. Components of the SSHI interface.

Symbol	Value (unit)	Description
Q_{LC}	4.4	Quality factor of resonant L-C_{P1}
R_{LC}	0.48 Ω	Equivalent resistor of resonant L-C_{P1}
q_{LC}	0.7	Inversion factor
L	10 mH	Resonant inductor in SSHI
C_r	4.7 μF	Regular capacitor in supply circuit
C_A	2.2 μF	Regular capacitor in supply circuit
C_B	2.2 μF	Regular capacitor in supply circuit
D_Z	15 V	Zener diode in supply circuit
L_f	700 mH	Low pass filter inductor
C_f	470 nF	Low pass filter capacitor

(IRF9640) pair for positive and negative switching. Table 4 shows the components used in the SSHI interface.

5.2 Experimental results

In this study, the experimental data validated the self-powered energy harvester for bicycle application and demonstrated the circuit operation. Fig. 15 shows the displacement, sensed velocity, switching signal, and piezoelectric voltage of the self-powered SSHI interface for acceleration of 2 m/s^2. Compared with the ideal waveform in Fig. 12(b), some switching noises were observed. These noises were from the switching action. When SSHI is active, high-frequency noise is easily introduced to the velocity control signal because the current-sensing resistance (R_C = 1 kΩ) is significantly lower than the output impedance of the piezoelectric element (the signal amplitude of the signal V_S is approximately 0.015 V). However, this noise does not influence the driving signal after the comparator (V_{cout}).

The operating limit of the self-powered technique is obtained when the comparator supplying DC voltage V_{CC} is lower than 2.5 V. A decrease in vibration magnitude results in a decrease in harvested power, thus reducing voltage V_{CC}. Therefore, the acceleration magnitude has a minimum value. Fig. 16 shows the experimental value of V_{CC} as a function of

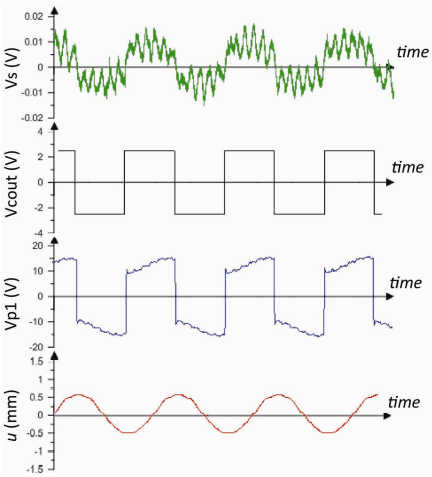

Fig. 15. Experimental waveform of the zero-velocity crossing detection circuit (velocity V_S, V_{Cout}, piezoelectric voltage V_{P1}, and beam tip displacement u).

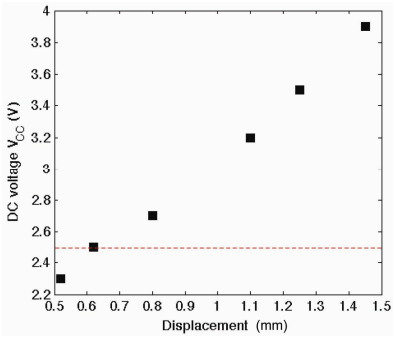

Fig. 16. DC voltage V_{CC} as a function of tip displacement.

displacement. DC voltage V_{CC} is equal to 3.9 V when the tip beam displacement magnitude is 1.45 mm and 2.51 V when the tip beam displacement magnitude is 0.62 mm. The experimental inferior limit of the system is 0.6 mm for V_{CC} to be greater than 2.5 V to power the circuit comparator.

In Fig. 17, sweeps of increasing frequency are plotted with an acceleration amplitude of 2 m/s^2 for the optimal resistive load R = 200 kΩ. The testing frequency ranges from 14 Hz to 25 Hz.

Experimental results for system harmonic excitations are obtained using the self-powered SSHI. The resonance frequency (f_{sh} = 18.77 Hz) is obtained when transducer output is shorted, whereas anti-resonance frequency (f_{op} = 18.8 Hz) is obtained when transducer output is open. Experiments show that maximum output power is reached near resonance. The use of the SSHI interface results in effective voltage inversion of transducer output every half-period and keeps the circuit open most of the time, resulting in open-circuit behavior. This behavior causes the maximum output power to occur near the anti-resonance frequency. Output power is dependent on excitation level and load resistance. Fig. 18(a) shows output power versus load resistance of two acceleration amplitudes, 2 and

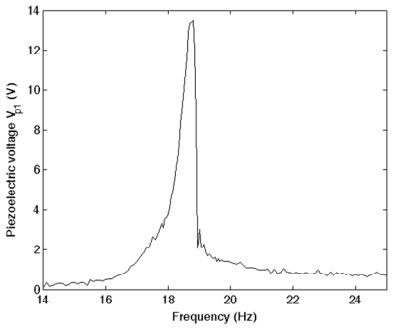

Fig. 17. Experimental frequency response result: acceleration 2 m/s^2.

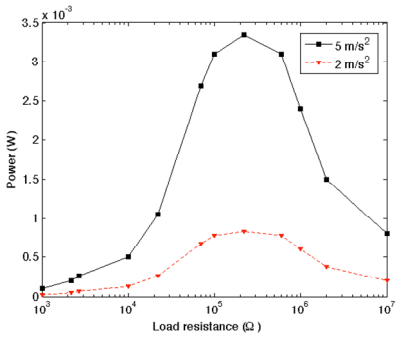

(a)

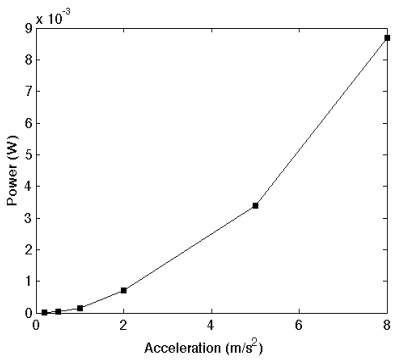

(b)

Fig. 18. (a) Output power as a function of load resistance at f = 18.8 Hz; (b) optimal output power as a function of acceleration at f = 18.8 Hz.

5 m/s^2. The optimum load is approximately 200 kΩ. The optimal output power versus acceleration at 18.8 Hz excitation is shown in Fig. 18(b). Output power is a function of the square of acceleration. The maximum output power is approximately 9 mW for an acceleration of 8 m/s^2. This amount of power is sufficient for a small on-board calculator.

6. Conclusion

Collecting ambient energy is a smart way of recharging or possibly replacing batteries in bicycle embedded devices (e.g., digital displays or wireless sensor nodes). Such power supply solutions improve device applicability and performance. In

this study, rolling-induced bicycle frame vibrations were investigated as an alternative power source. Detected bicycle vibrations show low spectral bandwidth. The largest amplitudes were found in the range of 2 Hz to 30 Hz. Thus, the harvester does not need broad frequency response. Piezoceramic elements glued to the cantilever beam convert mechanical energy to electrical energy. An electric interface is introduced to increase electromechanical conversion. A self-powered interface is achieved by integrating two additional piezoelectric patches; one patch senses velocity zero-crossing to drive switches of the SSHI circuit, whereas another provides a DC voltage source to supply electronic circuits. The power generator is tested on a shaker at the resonance frequency, and energy is harvested successfully, stored in the capacitor, and supplied to the electrical load. The results show that electric load power is 3.4 mW at R = 200 kΩ for a bicycle speed of 21 km/h on a paved track. However, harvested power is low for other bicycle speeds because fundamental frequency shifts at low bicycle speed. In this instance, utilizing a powerful vibration harvester with more cantilevers or with a nonlinear technique is recommended.

References

[1] W. Wang and O. A. Jianu, A smart sensing unit for vibration measurement and monitoring, *IEEE/ASME Transactions on Mechatronics*, 15 (1) (2010) 70-78.

[2] J. Park, S. Lee and B. Man Kwak, Design optimization of piezoelectric energy harvester subject to tip excitation, *Journal of Mechanical Science and Technology*, 26 (1) (2012) 137-143.

[3] D. Inman and S. J. Priya, Energy harvesting technologies, *Springer*, (2009).

[4] D. P. Arnold, Review of microscale magnetic power generation, *IEEE Transactions on Magnetics*, 43 (11) (2007) 3940-3951.

[5] L. Xie and R. Du, Harvest human kinetic energy to power portable electronics, *Journal of Mechanical Science and Technology*, 26 (7) (2012) 2005-2008.

[6] L. Tang, Y. Yang and C.K. Soh, Toward broadband vibration-based energy harvesting, *Journal of Intelligent Material Systems and Structures,* 21 (18) (2010) 1867-1897.

[7] A. Khaligh, P. Zeng and C. Zheng, Kinetic energy harvesting using piezoelectric and electromagnetic technologies-state of the art, *IEEE Transactions on Industrial Electronics*, 57 (3) (2010) 850-860.

[8] S. Roundy, P. K. Wright and J. Rabaey, A study of low level vibrations as a power source for wireless sensor nodes, *Computer Communications*, 26 (11) (2003) 1131-1144.

[9] D. Guyomar, A. Badel, E. Lefeuvre and C. Richard, Toward energy harvesting using active materials and conversion improvement by nonlinear processing, *IEEE Transactions on Ultrason., Ferroelectr., Freq. Control,* 52 (4) (2005) 584-595.

[10] E. Minazara, D. Vasic, F. Costa, G. Poulin and S. Tliba, Piezoelectric diaphragm for vibration energy harvesting, *Ultrasonics,* 44 (2006) 699-703.

[11] M. Ericka, D. Vasic, F. Costa and G. Poulin, Predictive energy harvesting from mechanical vibration using circular piezoelectric membrane, *Proc. of IEEE Ultrasonics Symposium*, Rotterdam, The Netherland (2005).

[12] Y. Y. Chen, D. Vasic, Y. P. Liu and F. Costa, Study of a piezoelectric switching circuits for energy harvesting with bistable broadband technique by work-cycle analysis, *Journal of Intelligent Material Systems and Structures,* 24 (2) (2013) 180-193.

[13] D. Vasic and Y. Yao, PWM interface for piezoelectric energy harvesting, *Electronics Letters*, 49 (13) (2013) 843-845.

[14] G. A. Lesieutre, G. K. Ottman and H. F. Hofmann, Damping as a result of piezoelectric energy harvesting, *Journal of Sound and Vibration,* 269 (2004) 991-1001.

[15] B. S. Lee, W. J. Wu, W. P. Shih, D. Vasic and F. Costa, Power harvesting using piezoelectric MEMS generator with interdigital electrodes, *Proc. of IEEE Ultrasonics Symposium*, New-York USA (2007).

[16] J. Liang and W. H. Liao, Impedance modeling and analysis for piezoelectric energy harvesting systems, *IEEE/ASME Transactions on Mechatronics*, 17 (6) (2012) 1145-1157.

[17] S. P. Beeby, M. J. Tudor and N. M. White, Energy harvesting vibration sources for microsystems applications, *Measurement Science and Technology*, 17 (12) (2007) 175-195.

[18] A. Badel, D. Guyomar, E. Lefeuvre and C. Richard, Piezoelectric energy harvesting using a synchronized switch technique, *Journal of Intelligent Material Systems and Structures,* 17 (8) (2006) 831-839.

[19] J. Liang and W. H. Liao, Energy flow in piezoelectric energy harvesting systems, *Smart Materials and Structures,* 20 (1) (2011) 015005.

[20] G. A. Lesieutre, G. K. Ottman and H. F. Hofmann, Damping as a result of piezoelectric energy harvesting, *Journal of Sound and Vibration,* 269 (3-5) (2004) 991-1001.

[21] Y. P. Liu and D. Vasic, Semi-passive Piezoelectric structural damping based on pulse width modulation switching circuit, *Journal of Mechanical Science and Technology,* 27 (12) (2013) 3625-3633.

[22] Y. C. Shu, I. C. Lien and W. J. Wu, An improved analysis of the SSHI interface in piezoelectric energy harvesting, *Smart Materials and Structures,* 16 (6) (2007) 2253-2264.

[23] Y. Y. Chen, D. Vasic, F. Costa and W. J. Wu, A self-powered switching circuit for piezoelectric energy harvesting with velocity control, *The European Physical Journal Applied Physics*, 57 (3) (2012) 30903.

[24] Y. Y. Chen, D. Vasic, F. Costa, W. J. Wu and C. K. Lee, Self-powered piezoelectric energy harvesting device using velocity control synchronized switching technique, *Proc. of IEEE IECON 2010*, Phoenix, Arizona, USA (2010).

[25] D. Vasic, Y. Y. Chen and F. Costa, Design of self-powering part of SSHI interface for piezoelectric energy harvesting, *Electronics Letters,* 49 (4) (2013) 288-290.

[26] Y. Y. Chen, D. Vasic, F. Costa, C. K. Lee and W. J. Wu, Self-powered semi-passive Piezoelectric structural damping based on zero velocity crossing detection, *Smart Materials and Structures,* 22 (2) (2013) 025029.
[27] E. Lefeuvre, A. Badel, C. Richard and D. Guyomar, Piezoelectric energy harvesting device optimization by synchronous electric charge extraction, *Journal of Intelligent Material Systems and Structures,* 16 (10) (2005) 865-876.

Dejan Vasic obtained his Agrégation, Master's, and Doctoral degrees in Electrical Engineering from Ecole Normale Supérieure de Cachan (France) in 1998, 2000, and 2003, respectively. He is currently an Assistant Professor of Electrical Engineering at the University of Cergy-Pontoise (France), where he is responsible for teaching sciences and technology in the master's degree program. His main research interests include piezoelectric materials for power electronics, DC-DC converters, energy harvesting, and structural damping.

Yu-Yin Chen received his joint Ph.D degree in Electrical Engineering from the National Taiwan University, Taiwan and from Ecole Normale Supérieure de Cachan, France in 2013. His research interests include vibration control, energy harvesting, piezoelectric transducer, and power electronics.

François Costa received his Ph.D. degree in Electrical Engineering from the University of Paris-Sud, Orsay, France, in 1992. He is also a Full Professor at the University Paris-Est Creteil, France, where he is responsible for teaching sciences and technology in the master's degree program. Since 1999, he has been the leader of the Power Electronics Team in the SATIE laboratory. His research concerns high-frequency medium-power converters, EMI issues and their modeling, HF instrumentation, integration in power electronics, and piezoelectric converters.